Bulletin of the Seismological Society of America, Vol. 97, No. 3, pp. 926–933, June 2007, doi: 10.1785/0120060152

Wave Gradiometry in the Time Domain

by Charles A. Langston

Abstract A time-domain approach for solving for the change in geometrical spreading and horizontal wave slowness in wave gradiometry is presented based on the use of the analytic signal. The horizontal displacement gradient of a wave is linearly related to the displacement and its time derivative. The coefficients of this relationship give the change of geometrical spreading, the change in radiation pattern, and horizontal slowness. The new time-domain technique incorporates estimates of the instantaneous amplitude and frequency of the three time series to solve uniquely for the wave-field coefficients. The analysis is simpler and more suited to fast array processing of displacement gradient data sets compared with a spectral ratio method.

Introduction

Wave gradiometry is a technique of using the spatial gradient of seismic wave fields to determine attributes of propagating seismic waves. It uses a very simple result from solutions of the wave equation to relate the spatial gradient of the wave to the time gradient (velocity) and original displacement itself (Langston, 2007a, 2007b). Simple propagating wave solutions to the wave equation that are useful in real data analysis can be generalized by considering a geometrical spreading function and horizontal slowness function that are functions of the spatial coordinates. For example, in one dimension a horizontally propagating wave can be represented by

$$u(t,x) = G(x)f(t - p(x - x_0)), \tag{1}$$

where p is the horizontal slowness, x_0 is a reference position, and $G(x)$ is the geometrical spreading function of the wave (Langston, 2007a). Differentiating equation (1) with respect to x gives

$$\frac{\partial u}{\partial x} = A(x)u + B(x)\frac{\partial u}{\partial t}, \tag{2}$$

where the coefficients $A(x)$ and $B(x)$ are given by

$$A(x) = \frac{G'(x)}{G(x)} \tag{3}$$

and

$$B(x) = -\left[p + \frac{\partial p}{\partial x}(x - x_0)\right]. \tag{4}$$

Equation (2) expresses a relationship between three different time series: the displacement derivative, and the displacement, and the displacement time derivative. The coefficients $A(x)$ and $B(x)$ represent the relative change in geometrical spreading and the horizontal slowness of the wave with position. These coefficients can be integrated to reconstruct the geometrical spreading and slowness:

$$\int_{x_0}^{x} A(x)dx = \ln\frac{G(x)}{G(x_0)} \tag{5}$$

$$p = -\frac{1}{(x - x_0)}\int_{x_0}^{x} B(x)dx. \tag{6}$$

Application of the technique of wave gradiometry involves first finding all three time series using 1D, 2D, or 3D arrays of sensors and then computing the wave coefficients. One-dimensional problems were considered in Langston (2007a) (article 1). Two-dimensional wave gradiometry involves the application of two 1D calculations (Langston, 2007b) (article 2). These references give several practical results with data applications for computing the wave-displacement derivatives using finite-difference techniques and then solving equation (2) for the coefficients using Fourier transforms and filter theory.

For example, the solution of equation (2) is mathematically straightforward if it is first transformed into the Fourier domain as

$$\hat{u}_{,x} = A(x)\hat{u} + B(x)i\omega\hat{u}. \tag{7}$$

Dividing through by the spectral displacement gives

$$\frac{\hat{u}_{,x}}{\hat{u}} = A(x) + i\omega B(x) \tag{8}$$

and

$$A(x) = \mathrm{Re}\left\{\frac{\hat{u}_{,x}}{\hat{u}}\right\} \tag{9}$$

$$B(x) = \frac{1}{\omega}\,\mathrm{Im}\left\{\frac{\hat{u}_{,x}}{\hat{u}}\right\}. \tag{10}$$

The coefficients can be found by calculating the real and imaginary parts of the complex spectral ratio of the displacement derivative and the displacement. This spectral ratio method was used in articles 1 and 2 by time windowing the displacement derivative and displacement seismograms, Fourier transforming, and working with equations (9) and (10) along with estimates of the mean and variances of the spectral ratios. However, it is well known that taking a spectral ratio (or deconvolution in the time domain) is fraught with problems, including window truncation effects, spectral nulls in the denominator, and other noise sources (Oldenburg, 1981; Langston and Hammer, 2001).

The purpose of this report is to present a time-domain method based on the analytic signal (Bracewell, 1978) to find the unknown coefficients $A(x)$ and $B(x)$ in equation (2), avoiding some of the pitfalls inherent in using spectral ratios. This method is motivated by some unresolved issues presented in Langston *et al.* (2006) involving computation of the horizontal phase velocity using the magnitude of the analytic signal (seismogram envelope). The issue concerned ignoring the phase of the original signals in forming the quotient. The phase determines the direction of wave propagation and is an essential part of gradiometry analysis. A full treatment of equation (2) using the analytic signal concept incorporates the phase and also gives an elegant method for determining the spatial coefficients in the time domain without recourse to matrix inversion or computation of spectral ratios. It is actually much more efficient and faster to implement than the moving time window spectral ratio method presented in articles 1 and 2. This theoretical development is complementary to the theory and results of articles 1 and 2 and only affects how the coefficients $A(x)$ and $B(x)$ are found in practice. All other theory and results are unchanged from the previous work.

Gradiometry Using the Analytic Signal

The analytic signal, $S(t)$ (Bracewell, 1978), is a generalization of Euler's relation for a complex exponential

$$e^{i\omega t} = \cos\,\omega t + i\,\sin\,\omega t = \cos\,\omega t - i\mathrm{H}[\cos\,\omega t] \tag{11}$$

such that for any real $s(t)$

$$S(t) = s(t) - i\mathrm{H}[s(t)], \tag{12}$$

where H[ ] is the Hilbert transform. Recall that the Hilbert transform of a function can be found through convolution by

$$\mathrm{H}[s(t)] = -\frac{1}{\pi t} * s(t) \tag{13}$$

and that the complex Fourier spectrum of the Hilbert transform of a function is shifted in phase by 90° (or a factor of i):

$$F\{\mathrm{H}[s(t)]\} = i\,\mathrm{sgn}\,\omega\,\hat{s}(\omega), \tag{14}$$

where,

$$\mathrm{sgn}\,\omega = \begin{Bmatrix} +1 & \omega \geq 0 \\ -1 & \omega < 0 \end{Bmatrix}. \tag{15}$$

Because the analytic signal is complex it may be represented in phasor form as

$$S(t) = |S(t)|\,e^{i\phi(t)} \tag{16}$$

where $|S(t)|$ is the envelope function or instantaneous amplitude, and in analogy to Euler's relation, the instantaneous frequency, $\omega(t)$, through

$$\omega(t) = \frac{d\phi(t)}{dt}. \tag{17}$$

In Langston *et al.* (2006), a dense linear array of strong-motion accelerographs was used to find horizontal phase velocity along the array using a plane-wave version of equation (2):

$$\frac{\partial u}{\partial x} = -p\,\frac{\partial u}{\partial t}. \tag{18}$$

The analysis consisted of computing the spatial derivative of displacement, $\partial u/\partial x$, using a simple forward difference between two accelerometers, finding the velocity, $\partial u/\partial t$, at one accelerometer, taking the envelope function of both to obtain $U_{,x}$ and $U_{,t}$, respectively, and computing the ratio to find the horizontal slowness through

$$p = \frac{|U_{,x}|}{|U_{,t}|}. \tag{19}$$

Although the numerical values for horizontal slowness computed this way agreed with values determined by phase move-out speeds, nevertheless, the use of the absolute value operations in equation (19) was *ad hoc* and ignored both the phase (positive or negative) of the original data and the pos-

sibility that waves may move in both directions along the array. In fact, this was observed for some coda waves.

Because the Hilbert transform and the analytic signal are linear operators, an exact solution for the coefficients $A(x)$ and $B(x)$ is possible using the concepts of instantaneous amplitude and frequency so that no *ad hoc* approximations like equation (19) are needed. First, we rewrite equation (2) for simplicity in notation by letting

$$u_{,x} = Au + Bu_{,t} \tag{20}$$

where the "comma" notation denotes differentiation with respect to x or t. Hilbert transform this equation, multiply it by $-i$, and add it to the original equation (20) to get the analytic signal version

$$U_{,x} = AU + BU_{,t}. \tag{21}$$

Because the Hilbert transform is a linear operator, we can use the relation

$$\mathrm{H}\left[\frac{\partial u}{\partial t}\right] = \frac{\partial}{\partial t}\,\mathrm{H}[u] \tag{22}$$

to obtain

$$U_{,x} = AU + B\,\frac{\partial}{\partial t}\,U. \tag{23}$$

Now the algebraic program is to represent each analytic signal in its phasor form, take the time derivative, inspect the real and imaginary parts of the result, and find the coefficients A and B. Proceeding, the phasor form is

$$|U_{,x}|e^{i\psi} = A|U|e^{i\phi} + B\,\frac{\partial}{\partial t}\left\{|U|e^{i\phi}\right\}, \tag{24}$$

where ψ and ϕ are the instantaneous phases of the displacement-derivative analytic signal and the displacement analytic signal, respectively. Taking the time derivative and using the chain rule gives an intermediate result

$$|U_{,x}|e^{i\psi} = A|U|e^{i\phi} + B\,\frac{\partial|U|}{\partial t}\,e^{i\phi} + B|U|e^{i\phi}i\,\frac{\partial\phi}{\partial t}. \tag{25}$$

The last term in equation (25) contains the instantaneous frequency of the displacement analytic signal (equation 17). Using

$$\phi(t) = \tan^{-1}\left[\frac{-\mathrm{H}[u(t)]}{u(t)}\right] \tag{26}$$

it is straightforward to differentiate this function to find the instantaneous frequency in terms of the original time function $u(t)$ as

$$\omega(t) = \frac{1}{|U|^2}\left\{\dot{u}(t)\mathrm{H}[u(t)] - u(t)\mathrm{H}[\dot{u}(t)]\right\}. \tag{27}$$

Manipulating equation (25)

$$|U_{,x}|e^{i(\psi-\phi)} = A|U| + B\,\frac{\partial|U|}{\partial t} + iB|U|\omega(t). \tag{28}$$

Equate the real and imaginary parts of the left-hand and right-hand sides. The real part is

$$|U_{,x}|\cos(\psi-\phi) = A|U| + B\,\frac{\partial|U|}{\partial t} \tag{29}$$

and the imaginary part is

$$|U_{,x}|\sin(\psi-\phi) = B|U|\omega(t). \tag{30}$$

Separating the real and imaginary parts this way gives two equations for the two unknown coefficients A and B with solutions

$$B = \frac{1}{\omega(t)}\,\frac{|U_{,x}|}{|U|}\,\sin(\psi-\phi) \tag{31}$$

and

$$A = \frac{|U_{,x}|}{|U|}\cos(\psi-\phi) - \frac{1}{\omega(t)}\,\frac{|U_{,x}|}{|U|^2}\,\frac{\partial|U|}{\partial t}\,\sin(\psi-\phi). \tag{32}$$

It's useful to consider a plane wave to get some physical insight into these results. If $G(x)$ is constant, then $A = 0$ and

$$U_{,x} = BU_{,t}. \tag{33}$$

In terms of the envelope and phase of these analytic signals

$$B = \frac{|U_{,x}|}{|U_{,t}|}\,e^{i(\psi-\gamma)}. \tag{34}$$

In addition to equation (31), if $A = 0$, equation (29) gives another relationship for B.

$$B = \frac{|U_{,x}|}{\dfrac{\partial|U|}{\partial t}}\cos(\psi-\phi). \tag{35}$$

Langston *et al.* (2006) used equation (34) in the data analysis without considering the instantaneous phase term $e^{i(\psi-\gamma)}$. Equations (31) and (35) are equivalent to (34) but are constructed with respect to the envelope and instantaneous phase of the displacement analytic signal rather than the velocity. The physical meaning of (34) is straightforward considering the nature of the displacement and time derivatives. For a forward-propagating plane wave (equation 18), $u_{,t}$ is proportional to $-u_{,x}$. Likewise, because of linearity, $U_{,t}$ is proportional to $-U_{,x}$, or the instantaneous phase difference must be π ($e^{i\pi} = -1$ in equation 34). Therefore,

$$p = -\frac{|U_{,x}|}{|U_{,t}|}\, e^{i\pi} = \frac{|U_{,x}|}{|U_{,t}|} \tag{36}$$

which is the relation used in Langston *et al.* (2006) and equation (19). For a backpropagating wave, $u_{,t}$ is proportional to $+u_{,x}$ so the relative instantaneous phase is zero. Thus,

$$p = -\frac{|U_{,x}|}{|U_{,t}|}\, e^{i0} = -\frac{|U_{,x}|}{|U_{,t}|}. \tag{37}$$

Obviously, the instantaneous phase must be considered to determine the directions of propagating waves.

A Theoretical Example

Equations (31) and (32) give a means for computing the gradiometry coefficients A and B in the time domain by using the analytic signals of the displacement derivative and the displacement. As defined, these coefficients are functions of space only, but because waves with differing geometrical spreading and horizontal slownesses may arrive at different arrival times, they effectively become functions of time when applied to signals with multiple wave arrivals. Figures 1 and 2 show the results of a wave simulation using these concepts. Three waves are assumed to be propagating in one dimension. Each is described as a Gaussian pulse with x^{-1} geometrical spreading but differing distance from the receiver, differing horizontal slownesses, and differing time lags (Table 1). Each wave is given by

$$u(t,x) = \frac{e^{-\alpha^2(t-px-\tau)^2}}{x} \tag{38}$$

and the sum of the three waves is shown in the figures. Equations (31) and (32) were used to determine coefficients A and B for this wave train assuming two realizations of the spatial derivative of $u(t,x)$. In the first, the exact spatial derivative was computed analytically and used to determine A and B. In the second, the central finite-difference operator discussed in article 1 was used to numerically compute the spatial derivative. A distance increment of 0.015 km (15 m) was used to be consistent with the data analysis in article 1. Appropriate computation of the distance derivative is major

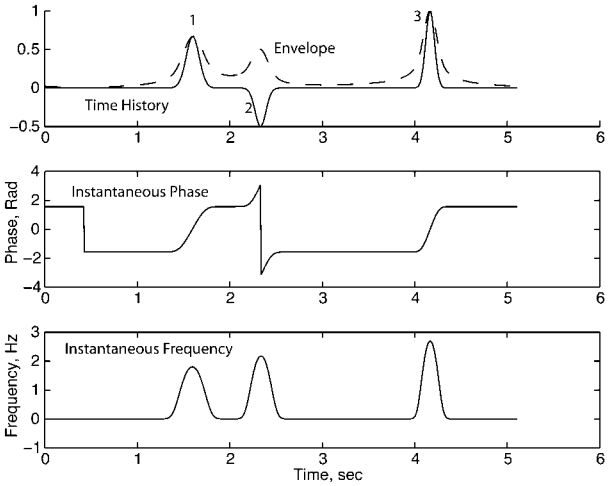

Figure 1. A theoretical example showing the time series of three separated waves (top panel) and resulting analytic signal attributes. The middle panel shows the instantaneous phase and the bottom panel the instantaneous frequency. Table 1 lists the parameters for the three waves.

topic in wave gradiometry but has been discussed in detail in articles 1 and 2.

Figure 1 shows the characteristics of the analytic signal for the sum of the three waves. The envelope function, instantaneous phase, and instantaneous frequency are quantities that go into the computation of the gradiometry coefficients. The instantaneous frequency (Farnbach, 1975) is particularly unusual compared with the usual spectral variety. Peaks of the instantaneous frequency coincide with peaks of the displacement and, in general, increase as the width of the Gaussian wave pulses decrease, a somewhat intuitive result.

Figure 2 shows the results for estimating the A and B coefficients using the exact and numerical spatial derivatives. The estimate for each coefficient at the time of each peak is shown and agrees well with the expected theoretical values. However, there are two effects that greatly influence the estimates of the A coefficient. The first can be seen in the third wave near 4 sec arrival time. This wave is well separated from the other two and displays the values expected for A and B using the exact spatial derivative. The numerical derivative, in contrast, introduces a linear trend with time for A and a shallow concavity in the peak for B. Numerical estimates of A and B at the peak arrival time are close to the actual values even though A varies by almost $\pm 50\%$ around the true value.

The second effect concerns the interference of two phases. Waves one and two between 1 and 3 sec arrival time are actually close enough to interact significantly within the analytic signal. The top panel in Figure 1 shows the envelope function for this time series. Because of the noncausality of the Hilbert transform, an impulsive phase is spread over all time according to equation (13). This is evident in Figure 1

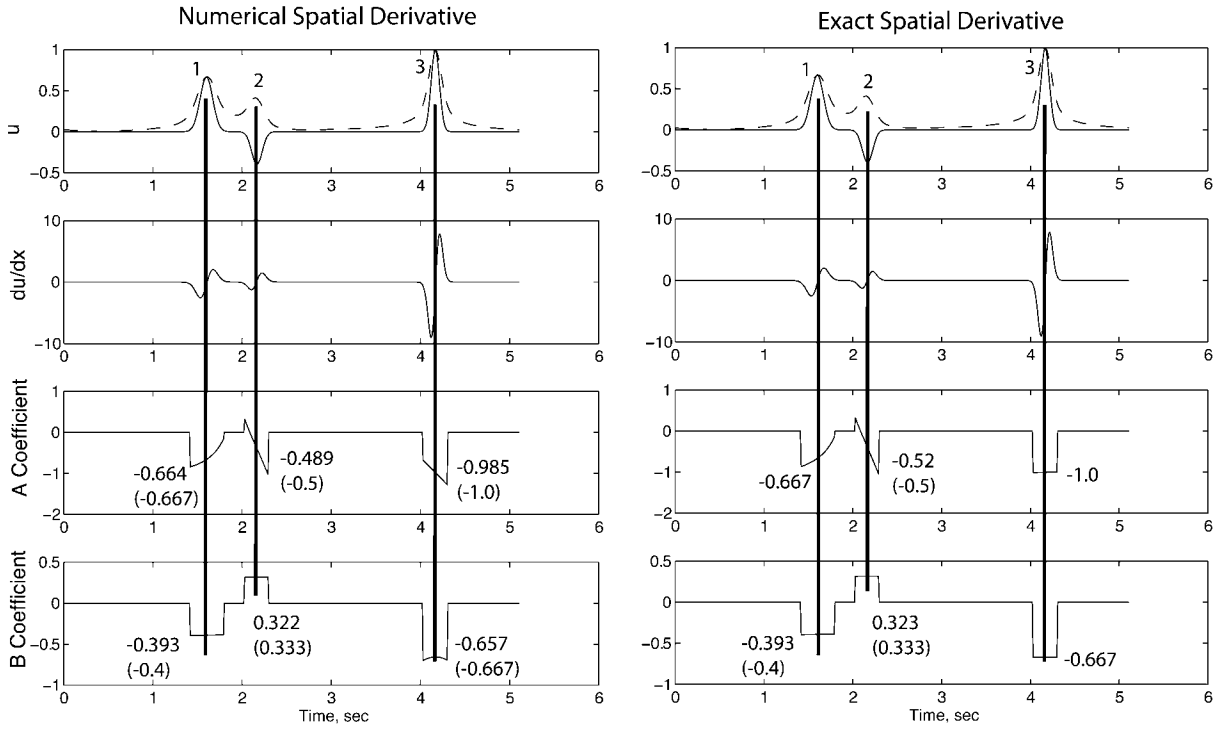

Figure 2. Evaluation of the gradiometry coefficients A (equation 32) and B (equation 31). The right-hand panel shows the theoretical result using the analytic displacement derivative. The left-hand panel shows the result after computing the displacement derivative from a numerical finite difference. The interference of waves 1 and 2 affects the determination for the A coefficient more than for the B coefficient. The effect of the numerical spatial derivative is most clearly shown by the distortions in A and B for wave 3. Values for the coefficients are given for the points at which the vertical lines cross. True values are in parentheses if the determined value is different from the true value.

Table 1
Parameters Used for the Wave Simulations

Wave	α (sec^{-1})	x (km)	Amplitude	p (sec/km)	τ (sec) Figs. 1 & 2	τ (sec) Fig. 3
1	10.	1.5	1	0.400	1.0	1.5
2	12.	2.0	−1	−0.333	3.0	3.5
3	15.	1.0	1	0.667	3.5	1.6

by the width of the envelope around each phase and significant envelope amplitude between these waves. This interference is manifest particularly in the A coefficient estimate by the smoothly varying trends. Even so, the estimates are quite close to the actual values at the peak arrival times using both the exact and numerical spatial derivatives.

The analytic signal formulation has additional problems when two waves interfere with each other. A careful examination of equations (31) and (27) shows that the instantaneous frequency has a singularity if the displacement envelope function has a zero. The B coefficient will also be singular if $\omega(t)$ has a zero. The A coefficient will be singular if the displacement envelope has a zero. In addition, if the displacement envelope has a zero the time derivative of the displacement envelope contained in the second term of equation (32) will have a step discontinuity at these time points. The algorithm that uses the analytic signal necessarily must find these isolated singularities in the various signals and avoid them.

Figure 3 shows an example of the same three waves undergoing harsh interference showing the effect of these singularities. The inferred A coefficient is quite complicated and, aside from the initial arrival, does not show the correct values for waves 2 and 3. The B coefficient for each wave is reasonably correct but the arrows point out a large, high-frequency excursion in both the A and B time series. This excursion comes from a zero in the instantaneous frequency.

The algorithm that was adopted to avoid these singularities incorporates the envelope of displacement time series and the instantaneous frequency. Two criteria were used to perform a coefficient calculation at a particular time point. The first criterion is that the level of the displacement envelope must be a small percentage of its maximum amplitude. The second criterion was that the level of the function in the curly brackets in equation (27) had to be a small percentage of its maximum amplitude. The percentage chosen

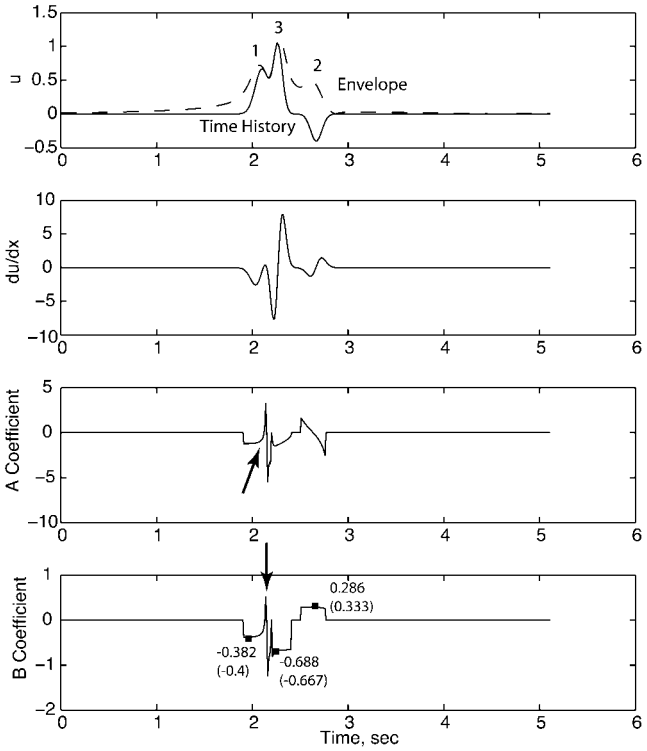

Figure 3. The three waves have been shifted in time to cause more interference between them (Table 1). The top panel shows the time series with the envelope function. Directly below is the exact spatial derivative followed by the *A* coefficient and the *B* coefficient on the bottom. The arrows denote the effects of singularities in the envelope and instantaneous frequency functions. The change in geometrical spreading (*A* coefficient) has significant biases due to the wave interference. However, a reasonable approximation of the horizontal slowness is recovered.

for both criteria was 0.1%. Increasing this number decreases the amount of signal analyzed by the method and is roughly equivalent, in effect, to the "variance" filtering concept used in articles 1 and 2.

Application to Field Data

This method was implemented in 1D and used to analyze a portion of the data set presented in Langston *et al.* (2006). Filtered array data from the strong-motion array that recorded ground accelerations from the first blast of the Embayment Seismic Excitation Experiment are shown in Figures 4 and 5. Please refer to Langston *et al.* (2005, 2006) for details of the experiment and the strong ground motion data set. These figures show the first 4 sec of the array vertical component waveforms filtered between 5 and 15 Hz. There are two coherent *P*-wave arrivals between 1 and 1.5 sec arrival time: the *P* head wave at the boundary of the unconsolidated embayment sediments and high-velocity Paleozoic sediments and the corresponding reflection. Each phase travels at a distinctly different horizontal phase velocity as measured by arrival-time differences across the array. Array elements were only 15 m apart and the entire eight-station linear array can be treated as a gradiometry array for frequencies less than 15 Hz (article 1).

Figure 4 shows the result for horizontal slowness. There is excellent time correspondence between the slowness estimates (in color) and the waveform peaks of the major phases. The horizontal phase velocity for the *P* head wave varies between 4.7 and 6.1 km/sec with an average of 5.04 km/sec. The horizontal phase velocity for the *P* reflection is lower at 2.23 km/sec (2.18 to 2.46 km/sec). These velocities are nearly identical with those obtained using the Fourier transform method in article 1. Note the regions in the *P*-wave coda that show a mixture of fast and slowly propagating waves moving across the array. Examples include an arrival at about 2 sec and at 2.7- to 3-sec times.

The change in geometrical spreading, the $A(x)$ coefficient, is shown in Figure 5. Again, the colored estimates associated with the two major phases show negative values consistent with amplitudes decaying with distance from the source. The *P*-wave coda shows a variety of relatively high-frequency negative and positive values that are reminiscent of the interference singularities observed in the theoretical examples previously.

It is interesting to compare results from the Fourier transform and analytic signal methods for finding the coefficients. Figure 6 displays a filtered *P* wave from station 5 (2.625 km) and the $B(x)$ coefficients obtained from the two methods. The spectral ratio method involves a moving time-window analysis where, in this case, a time window 0.4 sec long was shifted one eighth of its length along the seismogram. The data were windowed, the Fourier transform taken for the time window, and the spectral ratios formed to determine the coefficients (equations 9 and 10). In addition, "variance filtering" was performed to keep those estimates of the coefficients that were greater than twice the standard deviation of the real and imaginary parts of the spectral ratios. The result is shown in the middle panel of Figure 6. Computationally, the analytic signal method is at least two order of magnitudes faster because it involves only a few transforms of the displacement gradient and displacement time series to find the analytic signal, time derivative of the displacement envelope, instantaneous frequencies, and phases. Although there are some differences in the fine details of the coefficient determinations, Figure 6 shows that an additional drawback of the moving-window analysis is choosing the time point to assign the coefficient value. The midpoint is assumed here and, as a result, there is an apparent time advance in the coefficient value because of the relatively large time width of the window. This could be changed by assigning the coefficient to the end time of the window but the tremendous increase in speed afforded by the analytic signal method makes these adjustments unnecessary.

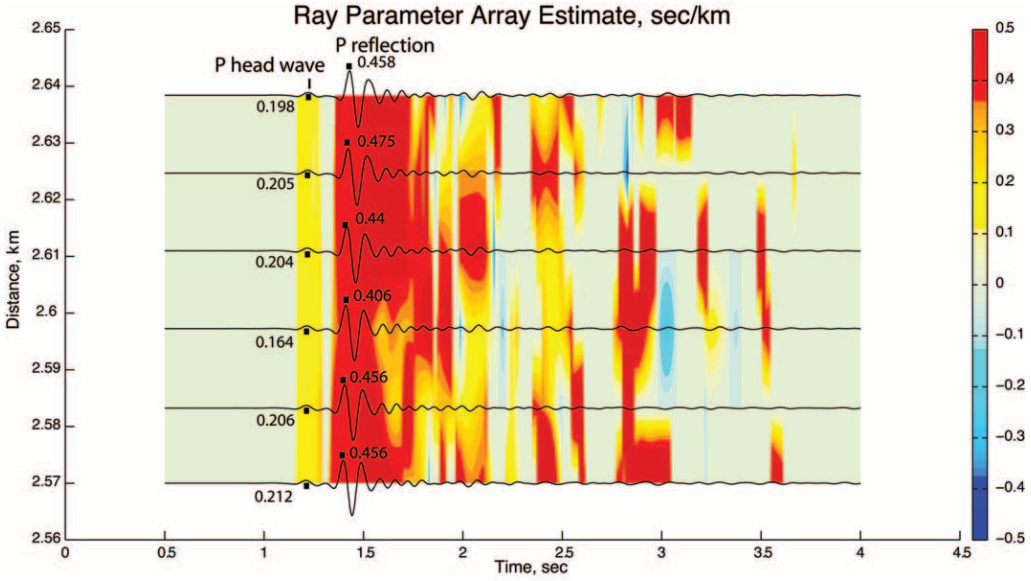

Figure 4. Application of the analytic signal method to field data to obtain the horizontal wave slowness. Vertical component seismograms from a large explosion recorded on a dense array of accelerometers are shown as the time series. The center six elements of the eight-element array are shown. The acceleration data were correct to displacement and bandpass filtered between 5 and 15 Hz to conform with the restrictions on horizontal wavenumber and the finite-difference approximation for computing the displacement derivative (see article 1). The principal phases are a *P* head wave from the top of Paleozoic carbonates under roughly 900 m of unconsolidated sediments and the postcritical *P* reflection from the same interface. The color-density plot shows contoured estimates of the horizontal slowness (ray parameter) for waves in this record section. Numerical values are also shown for selected arrivals.

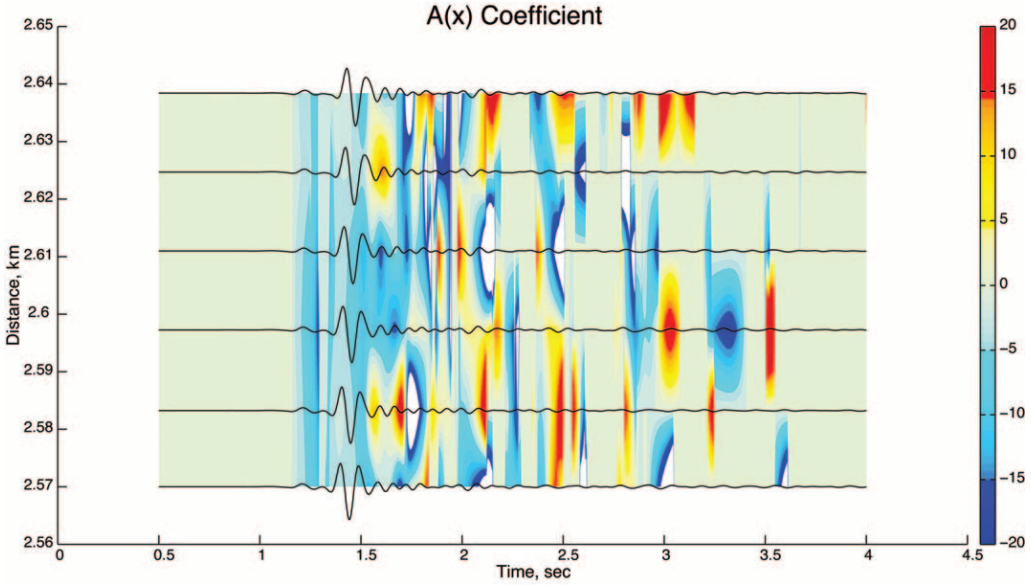

Figure 5. Application of the analytic signal method to field data to obtain the change in geometrical spreading across the array. Same scheme as in Figure 4. Small areas of white in the color density indicate values beyond the imposed color scale.

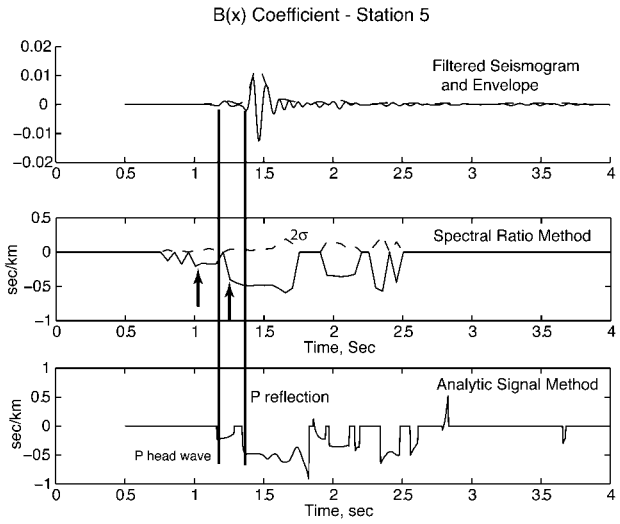

Figure 6. Comparison of the spectral ratio and analytic signal methods for obtaining horizontal wave slowness. Gradiometry analysis was carried out for station 5 (2.625 km on Figs. 4 and 5). The middle panel shows the result using the spectral ratio method. The dashed curve denotes twice the standard deviation of the estimate used in "variance filtering" to obtain the values of the coefficient as a function of time. The lower panel shows the analytic signal method result. The general features of the two methods are similar the values obtained for the *P* head wave and reflection are consistent. However, the vertical lines demonstrate that there is a time offset between the two methods because of the time-windowing process used in the spectral ratio method. See text for details.

Discussion

The full use of the analytic signal concept for the original relationship between the displacement derivative, displacement, and velocity of a wave gives a surprisingly straightforward way to solve for the geometrical spreading and slowness coefficients, clarifying the method suggested by Langston *et al.* (2006) for deducing horizontal phase velocity along a dense array. The theory has been developed for the 1D case but can be applied without change to the 2D analysis given in article 2. The 2D analysis requires the solution of two 1D problems in x and y, respectively, that are combined to find the wave azimuth, radial slowness, and change in radiation pattern across the array. Previous results involving filtering of the seismograms and applying a reducing velocity remain the same because the analytic signal is a linear operator. Discussion involving the errors in estimating the spatial derivatives from finite-differencing signals from array elements also remains the same. The Monte Carlo error analysis involved in determining errors in the 2D coefficients needs to be based on the means and variances of $A(x)$ and $B(x)$ in time rather than in frequency as used in article 2. This is beyond the purpose of the present article and will be the subject of future work.

Conclusions

Casting the gradiometry problem for a wave propagating in one dimension into a form that incorporates the analytic signals of the displacement gradient, displacement, and velocity yields a direct, time-domain solution for the gradiometry coefficients. There are isolated singularities in time for the coefficients due to the interference of waves that produce zeros in the envelope functions and the instantaneous frequency and step singularities in the time derivative of the envelope functions. These singularities can be avoided in an algorithm to obtain the change in geometrical spreading and horizontal slowness as a function of time for data collected in a gradiometry array. The analytic signal method is robust, is time-specific in associating a wave attribute to a particular time-domain arrival, and is computationally simpler and faster to implement than the spectral division method. The method is naturally applicable to 2D and 3D gradiometry arrays because these problems involve the solution of two and three 1D problems, respectively. This method is theoretically exact and clarifies an approximation used in Langston *et al.* (2006) for finding the horizontal slowness from a strong-motion gradiometry array.

Acknowledgments

This work was supported by the Mid America Earthquake Center through contracts HD-3 and HD-5. Paul Bodin reviewed an early version of this manuscript and suggested some useful changes. I also thank two anonymous reviewers and associate editor Fred Pollitz for their comments that were used to improve the manuscript. This is CERI contribution no. 509.

References

Bracewell, R. N. (1978). *The Fourier Transform and Its Applications*, McGraw-Hill Book Company, New York.

Farnbach, J. S. (1975). The complex envelope in seismic signal analysis, *Bull. Seism. Soc. Am.* **65,** 951–962.

Langston, C. A. (2007a). Spatial gradient analysis for linear seismic arrays, *Bull. Seism. Soc. Am.* **97,** 265–280.

Langston, C. A. (2007b). Wave gradiometry in two dimensions, *Bull. Seism. Soc. Am.* **97,** 401–416.

Langston, C. A., and J. K. Hammer (2001). The vertical component P-wave receiver function, *Bull. Seism. Soc. Am.* **91,** 1805–1819.

Langston, C. A., P. Bodin, C. Powell, M. Withers, S. Horton, and W. Mooney (2005). Bulk sediment Qp and Qs in the Mississippi embayment, Central U.S., *Bull. Seism. Soc. Am.* **95,** 2162–2179.

Langston, C. A., P. Bodin, C. Powell, M. Withers, S. Horton, and W. Mooney (2006). Explosion source strong ground motions in the Mississippi embayment, *Bull. Seism. Soc. Am.* **96,** 1038–1054.

Oldenburg, D. W. (1981). A comprehensive solution of the linear deconvolution problem, *Geophys. J. R. Astr. Soc.* **65,** 331–358.

Center for Earthquake Research and Information
University of Memphis
3876 Central Ave., Suite 1
Memphis, Tennessee 38152-3050

Manuscript received 4 August 2006.